THE JOURNAL OF PHYSICAL CHEMISTRY C
A JOURNAL OF THE AMERICAN CHEMICAL SOCIETY

pubs.acs.org/JPCC
Article

Exploring the Mechanism of the Electrochemical Polymerization of CO_2 to Hard Carbon over CeO_2(110)

Florian Keller, Johannes Döhn, Axel Groß, and Michael Busch*

Cite This: https://doi.org/10.1021/acs.jpcc.3c08356
Read Online

ACCESS | Metrics & More | Article Recommendations | Supporting Information

ABSTRACT: Conversion of CO_2 to hard carbon is an interesting technology for the removal of carbon dioxide from the atmosphere. Recently, it was shown that CeO_2 can selectively catalyze this reaction, but we still lack information regarding the reaction mechanism. Using density functional theory modeling, we explore possible reaction mechanisms that allow for the polymerization of CO_2. According to our computations, the reaction is initialized by the adsorption of CO_2 in an oxygen vacancy. Owing to the rich defect chemistry of ceria, a large number of suitable sites are available at the surface. C−C bond formation is achieved through an aldol condensation-type mechanism which comprises the electrochemical elimination of water to form a carbene. This carbene then performs a nucleophilic attack on CO_2. The reaction mechanism possesses significant similarities to the corresponding reactions in synthetic organic chemistry. Since the mechanism is completely generic, it allows for all relevant steps of the formation of hard carbon like chain growth, chain linkage, and the formation of side chains or aromatic rings. Surprisingly, ceria mainly serves as an anchor for CO_2 in an oxygen vacancy, while all other subsequent reaction steps are almost completely independent from the catalyst. These insights are important for the development of novel catalysts for CO_2 reduction and may also lead to new reactions for the electrosynthesis of organic molecules.

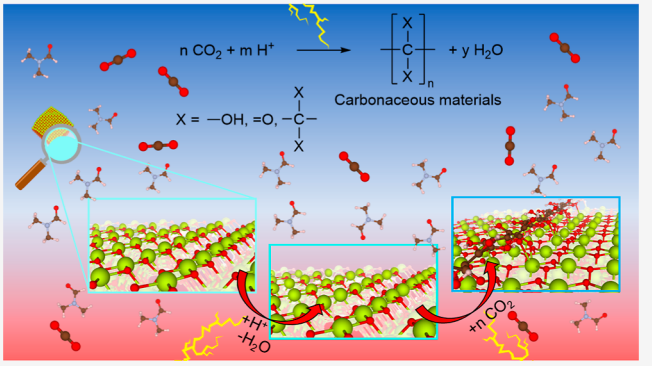

INTRODUCTION

With the increase in global greenhouse gas emissions,[1,2] an increasing number of severe consequences of global warming have become apparent in recent years. To minimize their impact on the world's population, it is crucial to find methods to effectively capture, convert, and store CO_2. A promising technology to achieve this is negative emission technologies (NETs).[3,4] NETs range from biological conversion of CO_2 into biomass through microorganisms,[5,6] algae,[5,6] or afforestation[7,8] to air capture followed by direct CO_2 storage[7,9] or chemical,[10,11] electrochemical,[5,6,8,12] and photoelectrochemical[13] conversion into long-term stable materials such as oxalates[14,15] or hard carbon[4] and carbon fibers.[16]

Unfortunately, chemical storage of CO_2 as oxalate requires high pressures, a sacrificial reducing agent and the introduction of a counterion such as Ca^{2+}[17,18] which renders them technically demanding. Similarly, other chemical and electrochemical routes for CO_2 conversion into nonvolatile products like the synthesis of hard carbon still face severe challenges. To complicate the situation even more, the methods currently considered for CO_2 reduction must be sustainable themselves[19] while at the same time scalable to convert several gigatons of CO_2 per year.[20] Accordingly, any meaningful process must rely on abundant materials and, in itself, be CO_2-neutral. Furthermore, to completely remove CO_2 from the atmosphere, it is insufficient to convert it into hydrocarbons or alcohols since their combustion again results in CO_2.[21,22]

Indeed, most processes for CO_2 reduction typically target precisely these products.[21,22] An example of this is the chemical synthesis of methanol from CO_2 and H_2 using Cu/Zn/Al[23−25] or In oxide[26] catalysts. For electrochemical CO_2 reduction on the other hand, a very diverse set of materials which includes both homogeneous[27−31] and heterogeneous[31−34] catalysts has been proposed. Typical examples of homogeneous catalysts are transition metals coordinated by porphyrin[35−42] or phthalocyanine.[43,44] However, these catalysts are again mostly selective for CO or post-CO products like methane or simple C_2 and C_3 compounds which are unsuitable for NETs. The same is also true for common heterogeneous catalysts like transition-metal-doped graphene[45,46] or metallic Cu.[47,48] Indeed, the formation of oxalates has only been reported for few materials like Hg[49]

Received: December 22, 2023
Revised: March 26, 2024
Accepted: March 26, 2024

or Pb[50] but the validity of some of these results was questioned recently.[51]

On the other hand, a catalyst which converts CO_2 electrochemically to hard carbon was, to the best of our knowledge, absent until the recent seminal work of Esrafilzadeh et al.[52] They found that liquid Galinstan (GaInSn alloy) in 2 M H_2O/*N*,*N*-dimethylformamide (DMF) selectively catalyzes the electrochemical reduction to hard carbon with a moderately high onset overpotential of −310 mV. However, the current remains far below 1 mA/cm^2 up to an overpotential of roughly −1.3 V.[52] Thus, it is fair to say that despite the very low reported onset potential, almost no CO_2 reduction takes place until a much lower potential is reached. The authors hypothesized that a Ce oxide is the active material but no proof was provided.[52] In addition to the nature of the catalyst, also the mechanism through which the reaction proceeds is so far unknown. Nevertheless, CeO_2 is a well-studied material which is exposed to CO_2 in many gas-phase heterogeneous reactions.[53,54] Symington et al.,[55] for example, reported that CO_2 mostly adsorbs as a carbonate. While this can be a problem under gas-phase conditions, mechanisms exist to activate carbonates under electrochemical conditions.[39,40]

In what follows, we will evaluate the reaction mechanism for the polymerization of CO_2 to carbonaceous materials over CeO_2(110) using density functional theory (DFT) calculations. Our computations indicate that CeO_2(110) possesses an oxygen defect-rich surface under reaction conditions. We will show that these defects are indeed central for its reactivity. C−C bond formation proceeds through a simple electrochemical aldol condensation-type mechanism. These results provide critical insights for the design of more efficient catalysts for the electrochemical reduction of CO_2 to hard carbon and may also inspire new reactions for electrosynthetic routes to organic compounds.

COMPUTATIONAL DETAILS

Surfaces. All DFT calculations were performed using the PBE[56] generalized gradient approximation (GGA) functional with Grimme D3 corrections[57−59] as implemented into the Vienna ab initio simulation package (VASP version 5.4.1).[60] To evaluate the validity of our results, also PBE + *U*-D3 calculations with a Hubbard U[61,62] were performed for selected cases. Following previous work,[63] a Hubbard U of 4.5 eV was used. However, if not stated explicitly otherwise, no semi-empirical Hubbard-U corrections were added. A detailed discussion on the benefits of using a GGA ansatz for these types of materials can be found in the Supporting Information.

The electronic wave functions were expanded in plane waves with energies up to 650 eV and the convergence threshold was set to 10^{-6} eV. Convergence of the electronic structure calculations was aided by adding a Gaussian smearing of 0.1 eV. Core electrons were approximated with projector augmented wave (PAW) functions.[64] The structure was considered converged if the Hellman−Feynman forces were below 10^{-2} eV/Å. The bulk structures were optimized using a 5 × 5 × 5 *k*-point set. 1 ×1 surfaces were calculated using a 6 × 6 × 1 *k*-point mesh, while the *k*-point sampling was reduced to 3 × 6 × 1 for the 2 × 1 slabs and to 3 × 3 × 1 for the 2 × 2-sized slabs. Conversion from electronic to Gibbs free energies was achieved by addition of constant corrections for zero-point energies and entropies using the values reported by Chan et al.[65] and Nørskov et al.[66] The numeric values of each contribution are summarized in the Supporting Information (Table S1).

Attempts to include solvent effects through implicit solvents failed owing to well-known instabilities in VASPsol[67−69] for cerium oxides.[70] We therefore attempted to obtain solvation energies by performing single-point computations using the SCCS model[71] implemented into CP2K (version: 9.1).[72] However, we were unable to converge the wave function. Similarly, attempts to obtain solvation energies using CANDLE[73] and GLSSA13[73−75] implemented into jDFTx (version: 1.7.0)[76] failed owing to severe instabilities in the wave functions for the GLSSA13 model which resulted in unphysical solvation energy differences of up to −150 eV between different intermediates. For CANDLE on the other hand, constantly similar unphysical solvation energies of the order of 0.1 eV were obtained. Naturally, these shortcomings could have been circumvented by using an explicit solvation model. The simplest way to include explicit solvation would have been the use of a microsolvation approach.[77] However, this model is static in nature and therefore cannot account properly for the highly dynamic nature of a solvation shell. Additionally, it also requires the placement of solvent molecules based on chemical intuition, which is far from trivial for most of the rather complex intermediates considered in this work. This leaves a full ab initio molecular dynamics (AIMD) ansatz as the only means for a proper explicit solvation model. Performing these computations is already for the much simpler metal−water interface nontrivial and expensive[78] and thus even less feasible for our significantly more difficult system consisting of a complex oxide with nontrivial adsorbates in a nonaqueous medium. This renders any attempt to perform AIMD simulations already for a single structure extremely demanding and is therefore unfeasible for the very large number of structures considered by us. Thus, we resorted to reporting the gas-phase energies. This is a common simplification in computational electrochemistry which still yields reasonable reaction energies.[46,79−84]

Acid Dissociation Constants. pK_a values of the carbonate species in DMF were computed using the isodesmic method[85−87] in combination with the recently introduced method to predict proton solvation energies in nonaqueous solvents.[87,88] For a detailed description of the methods and benchmarks, we refer the reader to our previous work.[87,88] Identical to these studies, the dissociation of formic acid (pK_a in water: 3.77[89]) was used as the reference reaction and the computed pK_a values (p$K_{a(comp)}$) were, following earlier work,[87] scaled to correct for shortcomings of the implicit solvation model using

$$pK_a = 0.75pK_{a(comp)} + 3.2 \quad (1)$$

The DFT computations necessary for the determination of pK_a values were performed using Gaussian 16 (Rev C.01)[90] with the M06-2X functional[91] and a 6-311++G** basis set with diffuse and polarization functions on all atoms. Structures were considered converged if no imaginary frequencies were present. Solvation effects were included through the implicit SMD[92] solvation model for water and DMF as implemented into Gaussian 16. Hydrogen was computed in the gas phase.

RESULTS AND DISCUSSION

Active Species. It is commonly assumed that CO_2 reduction proceeds through the direct activation of CO_2 at the catalyst.[93,94] However, recent computational work clearly

https://doi.org/10.1021/acs.jpcc.3c08356
J. Phys. Chem. C XXXX, XXX, XXX−XXX

showed that at least in some systems, direct CO_2 reduction is blocked by a very high activation barrier.[39,40] For these systems, bicarbonate (HCO_3^-) or carbonic acid (H_2CO_3) was identified as the most likely active species. Carbonic acid is coupled to CO_2 through a pH-independent equilibrium.[95]

$$CO_2 + H_2O \rightleftharpoons H_2CO_3 \quad (2)$$

The formation of bicarbonate on the other hand includes the release of a single proton which renders the reaction pH-dependent.[95]

$$H_2CO_3 \rightleftharpoons HCO_3^- + H^+ \quad (3)$$

Our computations indicate that the formation of H_2CO_3 through reaction 2 is endergonic by 0.72 eV in DMF. Furthermore, the pK_a of carbonic acid increases from 3.88 in water[95] to 18.6 in DMF (reaction 3). The second deprotonation step has an even higher pK_a value of 45.3. The trend toward significantly increased pK_a values in DMF compared to water for neutral acids is in good agreement with the significantly lower stability of protons and other charged species in aprotic nonaqueous solvents.[87,88,96] Overall, this clearly shows that only CO_2 is a possible reactant for the CO_2RR in DMF.

Active Site at CeO_2. Under ambient conditions, ceria (CeO_2) is the most stable form of cerium.[97,98] Experimental[99] as well as theoretical[100−102] studies agree that the stability of stoichiometric ceria surfaces decreases in the order (111) > (110) > (100) (see also Figure S13). However, the (111) surface is chemically mostly inert and does not allow for the formation of oxygen defects under CO_2RR conditions (see also Figure S13).[99−102] Also, we did not find any adsorption of CO_2 on the defect-free surface. This is opposed to the (110) surfaces which are known to have a strong tendency for oxygen defect formation.[103,104] Indeed, according to our computations, a significant number of oxygen vacancies are already present at rather high potentials of the order of −0.2 V (Figure 2).[83] Moving toward the experimental onset potential of −1.15 V vs SHE in acetonitrile, up to 25% of the surface oxygens are removed. Owing to the repulsion interaction between vacancies, the most stable configuration features oxygen vacancies which are not directly adjacent (Figure 2).

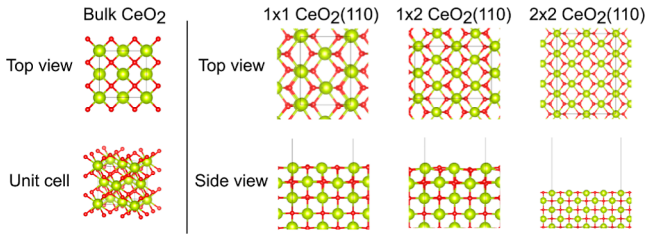

Figure 1. Depiction of bulk and surface arrangements of CeO_2. Ce: lime, C: brown, and O: red.

Overall, we find a rather high concentration of surface oxygen vacancies of 25% of which each in principle can act as a reaction center for CO_2 reduction. Accordingly, it is reasonable to assume that the chain growth starts at numerous spatially close oxygen vacancies simultaneously. Such a situation is most efficiently described by the rather small unit cell chosen by us which assumes 50% of the oxygen vacancies to be active reaction centers. Naturally, the surface could also undergo reconstruction. This effect was, however, neglected since under electrochemical conditions, a constant change of the surface due to dissolution and adsorption can occur. Thus, including these effects is computationally too demanding for an initial mechanistic study.

Reaction Mechanism. Building on the detailed analysis of the CeO_2(110) structure under reaction conditions and the identification of CO_2 as the sole reactant, it is possible to explore the detailed reaction path to form carbon chains of varying length. To reduce the computational efforts, all calculations for the chain propagation were performed for a (2 × 2) CeO_2(110) surface. Calculations using larger 3 × 3 and 4 × 4 supercells led to negligible changes in the vacancy formation energies, indicating a weak interaction between the vacancies in the 2 × 2 cell.

Exploring and understanding reactions which can result in C−C bond formations is the core of organic chemistry, and a huge amount of possible reactions have been discovered over the last 200 years. Accordingly, we nowadays have an excellent understanding of this chemistry.[105,106] Naturally, electrochemical routes to C−C bond formation possess some important differences compared with those typically used in synthetic organic chemistry. Probably the most important one is the fact that electrons with comparably high energy are easily available, which renders any redox chemistry feasible, even if it results in less common intermediates. Owing to this, any mechanistic consideration must also include more exotic intermediates like carbon or oxygen radicals (unpaired electron at the C or O atom) or carbenes (free electron pair at C atom). Nevertheless, these differences are too minor to fundamentally change the organic chemistry of C−C bond formation. We therefore opted to develop our initial candidate mechanisms by taking inspiration from standard reactions in organic chemistry like the Heck reaction,[107] the aldol condensation,[106] the pinacol reaction,[106] and the Wurtz reaction.[106,108] In addition to this, a mechanism featuring an unstabilized carbene has been included. A summary of all considered mechanisms and their relation to the original organic reactions can be found in the Supporting Information (Figures S1 to S12).

Chain Start. The initial step of any CO_2RR mechanism is the activation of CO_2. CeO_2(110) possesses a total of six potential adsorption sites and geometries (Figure 3). All attempts to adsorb CO_2 directly at either a formal Ce(III) or Ce(IV) site failed since CO_2 desorbed when attempting to bind the molecule through either carbon or oxygen. Accordingly, pinacol-style (Figures S4−S7) or Ce-catalyzed carbene-style (Figures S11 and S12) paths can be excluded. Furthermore, carbonate and single or double oxygen vacancies remain as the only potential active sites. This agrees with the common picture of CeO_2-catalyzed CO_2 reductions since high concentrations of oxygen vacancies facilitate the adsorption of CO_2.[109−111]

Let us start with the adsorption of CO_2 at a single vacancy site. This adsorption geometry is the initial step of the aldol-type (Figures S1−S3), Wurtz-type (Figures S8 and S10), Heck-type (Figures S9 and S10), and vacancy-catalyzed pinacol style-type (Figures S4−S7) paths. When binding CO_2 to this site, we indeed observe the typical signs of CO_2 activation like the reduction of the O=C=O bond angle from 180 to 145° and a C−O bond length increase from 1.17 to 1.20 and 1.25 Å, respectively. The C−O bond pointing toward the surface is slightly more elongated which reflects the interactions with one of the surface Ce ions. In line with this, the Ce−O distance of 2.88 Å, compared to 2.32 Å for a

https://doi.org/10.1021/acs.jpcc.3c08356
J. Phys. Chem. C XXXX, XXX, XXX−XXX

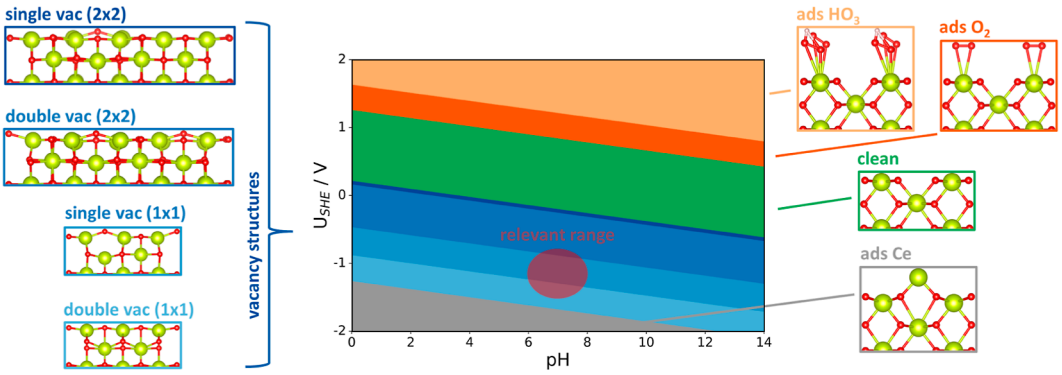

Figure 2. Computed Pourbaix diagram of the CeO_2(110) surface. The relevant surfaces under experimental conditions are marked by the violet area. Ce: lime, H: gray, and O: red.

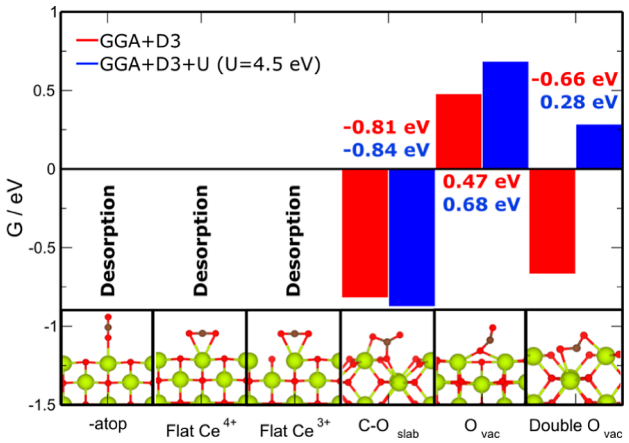

Figure 3. Summary of CO_2 adsorption sites and Gibbs free energies of adsorption over CeO_2(110). Red bars: PBE-D3; blue bars: PBE + *U*-D3 (*U* = 4.5 eV). Ce: lime, C: brown, and O: red.

bridged oxo (Ce−O−Ce) species, is still of a magnitude where some interactions can be expected. Additionally, also the OCO angle is reduced from 180° in the gas phase to only 145° which is a clear sign of activation. This is accompanied by a charge transfer of 0.4 electrons from the CeO_2(110) surface to the adsorbed CO_2. The adsorption of CO_2 into this site is somewhat endergonic by approximately 0.5 eV. It is interesting to note that this reaction becomes even more endergonic (0.7 eV) when a Hubbard-U correction is added to the PBE. The true value will most likely lie in between. Note that these unfavorable energetics do not necessarily result in a total inhibition of the associated reaction mechanism since the activation step in a vacancy is required to only occur once during the full mechanism. Thus, this only reduces the number of seed sites for the subsequent chain propagation.

Much more favorable energetics are observed for the adsorption if two adjacent oxygens are removed and a double vacancy is formed (up to ΔG = 1.2 eV). Under these circumstances, the chemisorption is exergonic by −0.7 eV for a pure GGA functional (Figure 3) while it becomes endergonic by 0.3 eV when a Hubbard-U correction is added. Similar to the adsorption in a single vacancy site, a significant activation of CO_2 is also observed here. For example, the C−O bond length is elongated to 1.26 and 1.31 Å while the O═C═O bond angle is at the same time reduced from 180° to only 125°. This adsorption geometry is accompanied by some interactions between the carbon and the adjacent Ce ion as indicated by the rather short Ce···CO_2 distance of 2.67 Å. In line with this activation, we also observe a charge transfer of 0.85 electrons from the surface to the adsorbed CO_2. The increased charge transfer is a direct result of the presence of 4 adjacent formal Ce(III) ions, which are able to donate electron density. However, the formation of adjacent oxygen vacancies is thermodynamically unfavorable (see Supporting Information) which renders this adsorption geometry unlikely.

The last stable CO_2 adsorption mode is the adsorption at a surface oxygen, which results in the formation of a surface carbonate. This path comprises the starting point for another pinacol-style path. This reaction is with −0.8 eV thermodynamically even more favorable than the adsorption in a double vacancy (Figure 3). A comparable value is also obtained with GGA + *U*. The high stability of surface carbonates is also in good agreement with earlier work targeted at gas-phase heterogeneous catalysis.[55] Identical to the two alternative adsorption modes, CO_2 bound in this fashion displays the typical signs of activation. e.g., the O−C−O bond angle is reduced to 126° while the C−O bond lengths are increased to 1.28 Å for the CO units pointing outward and 1.35 Å for the CO unit pointing toward CeO_2. In line with the adsorbate's apparent carbonate character, we also find very strong interactions with the adjacent Ce ions as indicated by the rather short Ce−O bond lengths of the order of 2.41 to 2.56 Å which compares favorably to a typical Ce−O−Ce single bond of 2.32 Å.

This structure can be converted electrochemically under water elimination to CO_2 in two consecutive PCET reduction steps (reactions 4 and 4).

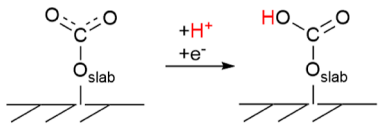

(4)

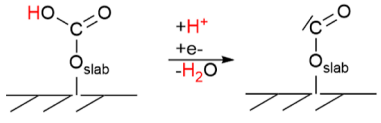

(5)

The product of this reduction reaction is structurally identical with a single vacancy-adsorbed CO_2. The first PCET step of the reduction mechanism (reaction 4) occurs a potential of 0.0 V vs SHE. This is opposed to the subsequent reductive elimination (reaction 4) which requires a very

https://doi.org/10.1021/acs.jpcc.3c08356
J. Phys. Chem. C XXXX, XXX, XXX−XXX

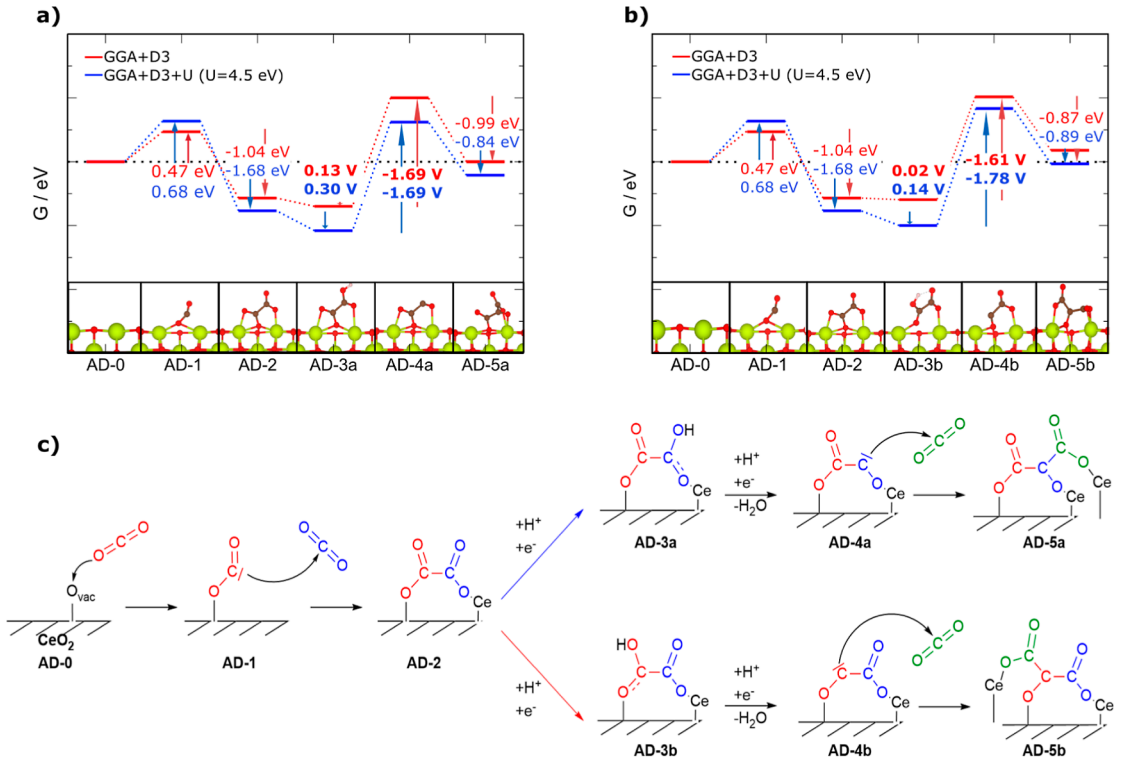

Figure 4. (a) Gibbs free energies of the initialization and chain propagation steps through the carbon not directly bound to the surface (path a). Red lines: PBE-D3; blue lines: PBE + *U*-D3 (U = 4.5 eV). (b) Gibbs free energies of the initialization and chain propagation steps through the carbon directly bound to the surface (path b). Red lines: PBE-D3; blue lines: PBE + *U*-D3 (U = 4.5 eV). (c) Schematic mechanism for the initialization and chain propagation steps. Ce: lime, C: brown, O: red, and H: gray.

negative potential of −1.5 V. This potential is slightly higher than the experimental onset potential[52] but still falls within the expected order of magnitude considering the error bars associated with our computations. Interestingly, we were only able to stabilize the vacancy-adsorbed CO_2 by putting CO_2 directly at the surface, while we observed its desorption when attempting to converge the structures coming from the carbonate intermediate. This could be indicative of a rather minor barrier which in turn would result in a fast equilibrium between dissolved and vacancy-adsorbed CO_2.

Overall, our computations indicate that only CO_2 attached through its oxygen atom to a CeO_2 vacancy is a reasonable starting point for CO_2 reduction. This adsorbed CO_2 configuration shows clear signs of activation. Thus, CeO_2 contributes to the initial activation step. All other considered configurations either are unstable (CO_2 bound through the carbon atom) or chemically inert (surface carbonates) or require a significant surface reconstruction (double vacancy-bound CO_2).

Chain Propagation. Once CO_2 has adsorbed at the surface, the chain can grow by reacting with additional CO or CO_2. As discussed above, the formation of surface carbonates comprises a highly favorable and likely intermediate. In terms of chain propagation, it is the starting point for a pinacol-style C−C coupling reaction between two adjacent surface carbonates. Our computations indicate that this mechanism is unlikely since no formation of a stable C−C bond could be achieved. This is indeed not surprising when considering that carbonates are chemically inert and do not possess a free electron pair at the carbon, which is a prerequisite for this reaction.

Thus, only single vacancy-bound CO_2 is a reasonable starting point. This leaves aldol, Wurtz, Heck, or vacancy-catalyzed pinacol-style reactions as possible routes for hard carbon formation. A Wurtz-style reaction can be excluded immediately since this path would require the presence of two adjacent CO_2 molecules adsorbed at oxygen vacancy sites (see Supporting Information, Figure S9 for details). This vacancy configuration is, according to our computations, energetically unfavorable (see Supporting Information). Accordingly, also the presence of two adjacent CO_2 is unlikely. Naturally, this also excludes a vacancy-catalyzed pinacol-style reaction which has a similar structural requirement. Furthermore, we do not find any stable configuration for a Heck-style coupling of a dissolved CO_2 with a vacancy-bound CO_2. This is indeed not surprising when considering that C−Ce bonds in CeO_2 are unstable owing to the high oxophilicity of Ce.[95,112]

Accordingly, only the aldol condensation-type mechanism remains as a possible reaction path. A summary of the initial steps for C−C bond formation assuming CO_2 as a reactant and the subsequent chain propagation is shown in Figure 4. C−C bond formation is achieved in an Eley−Rideal-type mechanism through the reaction of a vacancy-adsorbed CO_2 with a dissolved CO_2 (see also reaction from AD-1 to AD-2 in Figure 4).

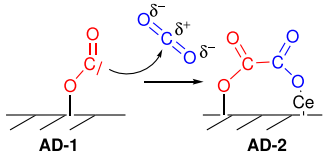

(6)

This step is strongly exergonic by approximately −1.0 eV (PBE-D3) and −1.7 eV (PBE + *U*-D3) which renders it thermodynamically highly favorable (Figure 4). The very high

https://doi.org/10.1021/acs.jpcc.3c08356
J. Phys. Chem. C XXXX, XXX, XXX−XXX

gain in energy can be understood from a detailed analysis of the electronic structure of AD-1. At first glance, this intermediate has significant similarities to an ordinary carboxylate (R, COO^-) group. e.g., it consists of a carbon with formally three bonds to two oxygen atoms. For a normal CO_2RR, this structure would be stabilized by a fourth bond to a metal center.[39,40,47,66] However, in the present case, the C−Ce distance of 2.88 Å indicates the absence of a strong covalent bond. This is also confirmed by the density overlap region indicator (DORI; Figure 5 AD-1) and electron

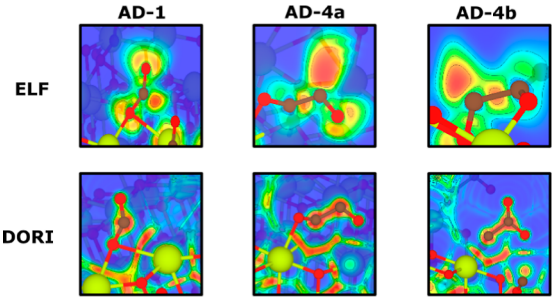

Figure 5. DORI and ELF plots of central intermediates are depicted. Ce: lime, C: brown, and O: red.

localization function (ELF; (Figure 5 AD-1) plots. The former is characterized by the absence of a localized basin between Ce and C which is a clear sign of the absence of a covalent bond between both atoms.[79,113] Furthermore, ELF indicates the presence of a localized electron pair on the carbon atom. This is also confirmed by the partial density of states (PDOS) which only show signs of a weak π-complex that interacts through the C═O double bond with Ce. This is indicated by the overlap of the O, C, and Ce bands close to the Fermi level (Figure 6a).

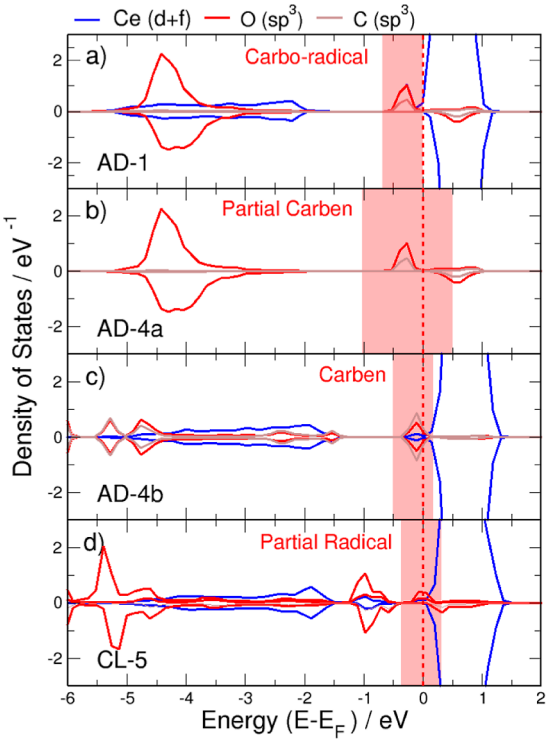

Figure 6. Spin-polarized PDOS plots of the crucial CO_2RR intermediates.

The interacting orbital is only occupied by a single α-spin electron, which renders it at least a partial radical. However, the corresponding unoccupied β-spin orbital is energetically very close. Thus, this orbital can easily become occupied when applying an electrochemical potential of less than −1.0 V vs SHE through an electron transfer from bulk CeO_2.

Note that both states are, even in the absence of an electrochemical potential, possible resonance structures. Chemically speaking, this state corresponds to a poorly stabilized carbene or carbon radical that is characterized by a free electron or electron pair at the carbon. These intermediates are highly reactive[106] which is in line with the observed very exergonic reaction energy. In what follows, we will, for the sake of simplicity, refer to reactive carbons of this or similar electronic structures as "carbenes".

The purely chemical C−C bond formation is followed by the stepwise electrochemical reduction of the C═O unit (AD-2 to AD-3a or AD-3b in Figure 4) and its elimination as water (AD-3a/AD-3b to AD-4a/AD-4b in Figure 4). Hydrogenation and water elimination may occur at either C_1 (CO_2 group anchored in the CeO_2 oxygen vacancy; lower path in Figure 4c) or C_2 (newly attached CO_2 group; upper path in Figure 4c). The first reduction step occurs in both cases already at a slightly positive potential between 0.0 and 0.1 V vs SHE and is therefore unproblematic at the potentials applied for CO_2 reduction (Figure 4). Comparable energetics are also obtained with GGA + U. The subsequent water elimination step on the other hand requires in both cases a very negative potential of approximately −1.7 V vs SHE which corresponds to the lowest redox potential observed in the reaction mechanism. Thus, at least a potential of this magnitude must be applied to allow all electrochemical steps to proceed, i.e., this reaction is potential-determining (for details see Supporting Information eq 8).[66,114,115]

At this potential, water would also be reduced to hydrogen. However, even in water (pH 7), the onset for hydrogen evolution over CeO_2 is of the order of approximately −1.3 V vs SHE.[116] Furthermore, the reaction is performed in DMF with minor amounts of water.[52] Accordingly, this side reaction is at least to some degree suppressed. The presence of this very negative reduction potential is not unexpected when considering the detailed electronic structure of the products, which is similar to the carbene in AD-1. Identical to this structure, we also observe for AD-4a and AD-4b the typical signs of a highly reactive carbon radical and/or carbene in the ELF (Figure 5 AD-4a and AD-4b). Additional support for this interpretation is also found in the PDOS plots (Figure 6b,c). Note that for AD-4b, again some indications for weak interactions with Ce are present, which points toward a weak π-complex-type interaction. However, no indications for a strong covalent C−Ce bond are observed in the DORI plot (Figure 5 AD-4a and AD-4b). No indication of comparable interactions is observed for AD-4a. Almost identical energetics are also obtained when applying a Hubbard U to Ce.

Note that the onset potential predicted by us is with −1.7 V vs SHE significantly larger than the −1.15 V vs SHE found by Esrafilzadeh et al.[52] However, it must be cautioned that the authors decided to report an onset potential at which almost no current density is observed rather than following the more common approach to report an overpotential to reach a defined current density.[117,118] Indeed, the current density remains far below 1 mA/cm^2 until a much lower potential of roughly −1.8 V vs SHE is reached. This very low current is a

https://doi.org/10.1021/acs.jpcc.3c08356
J. Phys. Chem. C XXXX, XXX, XXX−XXX

clear indication that the overall reaction is rather inefficient at lower overpotentials. Our computations on the other hand indicate that no reaction should take place at the experimental onset potential. A likely explanation for this discrepancy is the presence of impurities which interfere with the mechanism and allow for an additional stabilization of the carbene. This in turn would allow for the lower experimental onset potential albeit only at very low current densities. Indeed, Ag is known to leak from the "leakless" Ag^+/Ag-reference electrode[119] used by Esrafilzadeh et al.[52] C−Ag bonds are well-known motives in organometallic chemistry.[112] This beneficial contribution of trace amounts of impurities is not uncommon and has been observed in many other cases.[82,119−121] Such a mechanism would also be in good agreement with the observed very low current density at lower overpotentials, which in this case would effectively be limited by the amount of available silver and its diffusion to the electrode. In addition to this, our computations also do not include solvation effects which would stabilize the eliminated water molecule by −0.24 eV (Gaussian16/M06-2X/SMD) compared to our gas-phase reference. This in turn would shift the onset potential toward a less negative value. Furthermore, protons are destabilized by approximately 0.7 eV in DMF compared to water.[87,88] Including these effects would increase the onset potential to a value of approximately −0.9 V.

Once the carbene species in AD-4a or AD-4b has been formed, C−C bond formation again takes place through an Eley−Rideal-type reaction step in which a nucleophilic attack at a dissolved CO_2 atom takes place. This allowed the chain to grow by an additional C_1 unit. In line with the very high reactivity of a carbene species, this step is strongly exergonic by roughly −0.9 eV for both pure GGA and GGA + U independent of whether CO_2 is attacked from a carbene at C_1 or C_2. From here, the polymerization mechanism proceeds by repeating the previous steps. e.g., a reactive carbene intermediate is formed through the reduction of a C═O unit and water elimination followed by its attack on a dissolved CO_2. Naturally, chain propagation could also proceed through a Langmuir−Hinshelwood-type mechanism rather than the above-described Eley−Rideal-type path. This alternative route would require the adsorption of CO_2 in a vacancy prior to forming a C−C bond. However, CO_2 adsorption in an oxygen vacancy is somewhat endergonic and therefore less favorable (see Figure 3) while the Eley−Rideal-type C−C bond formation is strongly exergonic. Thus, prior activation of CO_2 through adsorption at the surface seems unnecessary.

Overall, the proposed mechanism requires CeO_2 only as an anchor for the initial adsorption of the first CO_2. Beyond this point, the reaction becomes surprisingly independent of the catalyst. Accordingly, also later oligo- and polymerization steps can proceed without the need for interactions with the catalyst provided an electron transfer from the cathode to the terminating carboxylate (R−COO) group is feasible and CO_2 is still available as feedstock. This sets CeO_2 apart from classical CO_2 reduction catalysts which contribute more directly to the reaction path by stabilizing the carbene intermediates through a metal−carbon bond[47,122] and adsorption sites for the coupling partner.[47] Once the chain has grown through subsequent reactions with CO_2, the reduction and conversion of the keto group into their enol

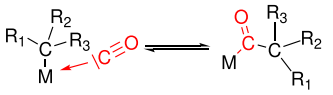

(7)

form becomes possible. This results in the formation of an energetically favorable conjugated π-electron system. The obtained conjugated π-electron system allows for the stabilization of the carbene which in turn makes subsequent water elimination steps energetically even more favorable.

An important variation of the above mechanism is to assume CO as feedstock. CO may, for example, be formed in situ through reduction of CO_2. In this case, the chain growth becomes purely chemical. e.g., the only required reaction steps are the nucleophilic attack of the carbene at a dissolved CO. In contrast to the attack on CO_2, this reaction is only thermoneutral. This is not unexpected when considering that the highest occupied molecular orbital (HOMO) in CO is a carbon-centered σ* antibonding orbital which places significant electron density at the carbon.[112,123] Accordingly, CO is a very poor electrophile. Indeed, chain propagation through reactions with CO typically proceeds through a migratory insertion in which CO binds to the catalyst prior to forming a C−C bond (reaction 7).[112]

In the present case, no such interaction with the catalyst is possible owing to the oxophilicity of Ce and the steric constraints of the Ce centers for which all free valences are already saturated. This renders such a variation of the mechanism of the PEG model highly unlikely.

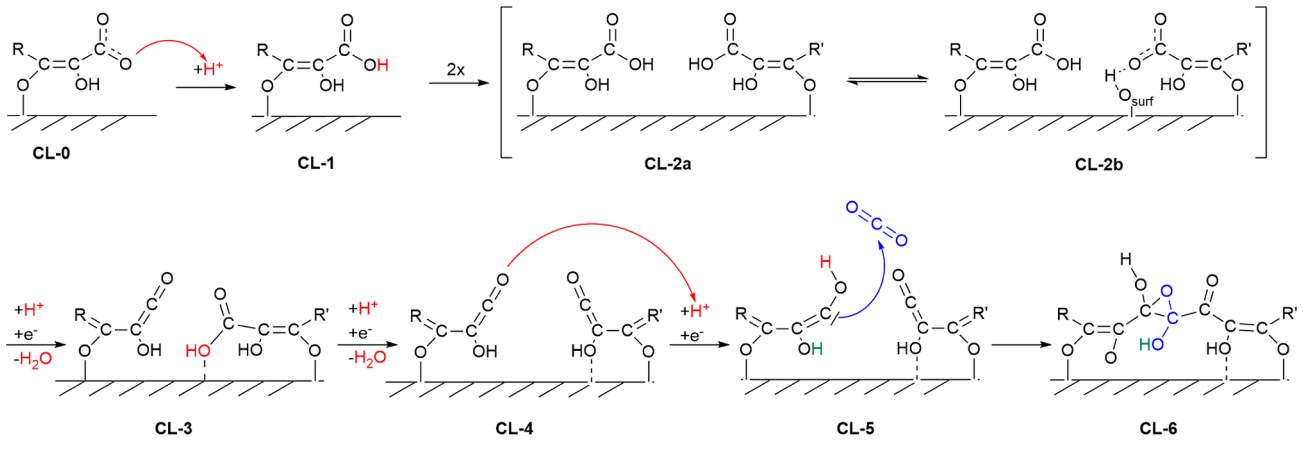

Figure 7. Schematic summary of the most likely reaction mechanism for the linkage of two olefin chains.

https://doi.org/10.1021/acs.jpcc.3c08356
J. Phys. Chem. C XXXX, XXX, XXX−XXX

Chain Linkage. The chains formed during the propagation steps may at some point meet and link with other olefin chains. To evaluate possible chain linkage mechanisms, a model system whose unit cell was doubled along the *x*-axis was constructed (see Figure 1). This reduces the strain within the olefin chain and thus corresponds to a more realistic situation. Owing to the rigidity of the chosen model system, no movements of the, in principle, rather flexible carbon chains are possible. This is justified in the present case, since this flexibility only affects the probability of 2 chains to meet but not the underlying chemistry of chain linkage. Furthermore, all keto groups were reduced to their enol form since this allows for the formation of a long and energetically favorable conjugated π-electron system.

Identical to the previous chain propagation steps, the chain linkage is also initialized by the reduction of two terminal R−COO$^{\bullet}$ groups to two carbonic acids (R−COOH; reaction from CL-1 to CL-3 in Figure 7). Both reaction steps are energetically highly favorable as indicated by the rather high reduction potentials of −0.2 and 0.7 V vs SHE (Figure 8).

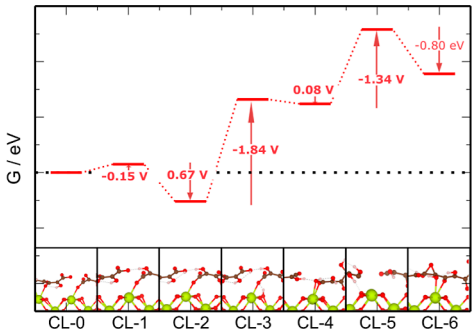

Figure 8. Energetics of the chain linkage mechanism. For the detailed mechanism, see Figure 7. The reaction energies were obtained using a pure PBE-D3 functional. Ce: lime, C: brown, O: red, and H: gray.

Note that during the second step, a proton transfer from the R−COOH group to a surface Ce−O−Ce oxo site occurs. This allows for a much more stable configuration and thus results in a positive potential for the second reduction reaction. Overall, both steps are unproblematic under reaction conditions. The subsequent reductive elimination through release of water (reaction from CL-3 to CL-5 in Figure 7) is thermodynamically significantly more demanding as indicated by the very negative potential of −1.8 V vs SHE for the first water elimination. This value is comparable to what has been observed for earlier water elimination steps (compare with Figure 4). The slight decrease of the potential by approximately −0.2 V might be the result of having to break a rather strong hydrogen bond (d(HO···HO) = 1.78 Å) between the carboxylic acid OH group and an adjacent alcohol. As a part of this elimination step, the opposite carboxylic acid group rearranges by transferring the proton back from the surface Ce−OH−Ce group to the R−COO^{-} group. In addition to this, a strong hydrogen bond between the OH group of the carboxylic acid and an alcohol at the opposite chain is formed [d(HO···HO) = 1.65 Å]. The second water elimination in contrast occurs already at a much higher potential of only 0.1 V vs SHE.

In principle, chain linkage could now proceed through a simple CO_2 insertion. However, our computations show that this reaction is thermodynamically unfavorable. e.g., the direct chain linkage is endergonic by 1.5 eV. At first glance, this may seem surprising when comparing it to the very exergonic C−C bond formation steps during the chain propagation phase. However, this result can be rationalized by the marked differences in the electronic structure. The first and probably most important difference is the fact that the newly inserted carbon atom possesses an sp^3 hybridization and thus is not part of a delocalized π-electron system. Accordingly, two formal radical C−O$^{\bullet}$ groups are obtained. One of these groups is stabilized through a proton transfer from an adjacent alcohol which itself is oxidized to a ketone. In addition to this, the chain rearranges such that the C−OH bond is weakened (bond elongation from 1.31 Å for an alcohol to 1.58 Å). This configuration is stabilized by a Ce−OH interaction [d(Ce−O) = 2.53 Å] and a strong hydrogen bond to the second adjacent alcoholic group [d(HO···HO) = 1.53 Å]. This allows the second C−O$^{\bullet}$ radical to form at least a partial C=O double bond (see Supporting Information). However, the very long C−O bond length of 1.30 Å, which is close to the bond length observed for an alcohol, suggests that the oxygen is still mostly of a radical nature.

In addition to this, the terminal C_2O groups form linear ketene derivatives ($R_2C{=}C{=}O$) where one of the C−R bonds corresponds to the enol chain and the second R to an OH group. While ketenes themselves are highly reactive,[105,106,124] they generally react as electrophiles, e.g., they accept an electron pair.[125] No such reaction is possible with CO_2 which is owing to the very stable C=O double bonds unable to provide an electron pair. This is opposed to CO which can donate its lone pair to form C−C bonds with both ketene groups and thus link both chains. In addition to this, the inserted CO forms a ketone rather than an unstable "double radical". In line with this, CO insertion is energetically extremely favorable by −5.2 eV. Note that this very strong exergonicity is not unexpected since CO is inserted between two extremely reactive functional groups under formation of two new C−C bonds.

A more likely reaction route in the absence of CO would be chain linkage through a [2 + 2] cycloaddition of two ketenes which mostly results in the formation of 4-membered cyclic esters (β-lactones; reaction 8).[105,126−131]

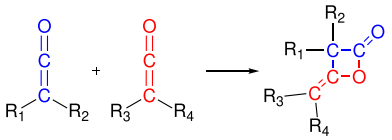

(8)

This ester could, in turn, be converted into an olefin through a simple ester hydrolysis (reaction 9).

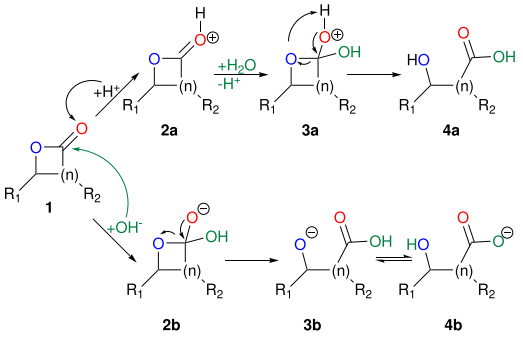

(9)

https://doi.org/10.1021/acs.jpcc.3c08356
J. Phys. Chem. C XXXX, XXX, XXX−XXX

For many ketenes, such a reaction can already proceed at room temperature.[105,106,124,126,127] A similar [2 + 2] cycloaddition between ketenes and CO_2 is in principle possible under elevated temperature or irradiation but typically too slow to be of relevance for chain propagation or chain linkage.[132]

These reactions are impossible in the present case, owing to the limited flexibility of our model system. Instead, the ketene is reduced to a R_2−C═C−OH species at a rather negative potential of −1.34 V vs SHE (CL-4 to CL-5 in Figure 7). This converts the terminal carbon again into a highly reactive intermediate. According to the PDOS (Figure 6d), it is similar to the initial carbene of AD-1, characterized by a singly occupied C−O with the unoccupied β spin being very close in energy. In line with this, we observe the usual characteristics of a free electron or electron pair in the ELF (see Figure 9).

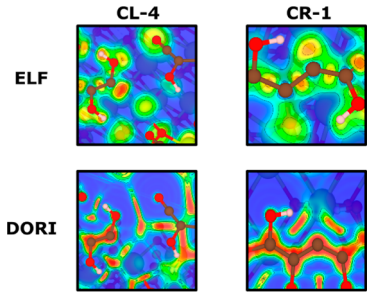

Figure 9. DORI and ELF plots of central ketene intermediates CL-5 and CR-1 in Figures 7 and 10. Ce: lime, C: brown, O: red, and H: gray.

According to the DORI and the PDOS, this carbene seems to be somewhat stabilized through interactions with Ce (Figures 9 and 6d). Thus, the electronic structure is again best described by a superposition of the radical and carbene mesomeric structures. The obtained carbene is finally sufficiently reactive to allow for the insertion of CO_2 through a nucleophilic attack (reaction 10).

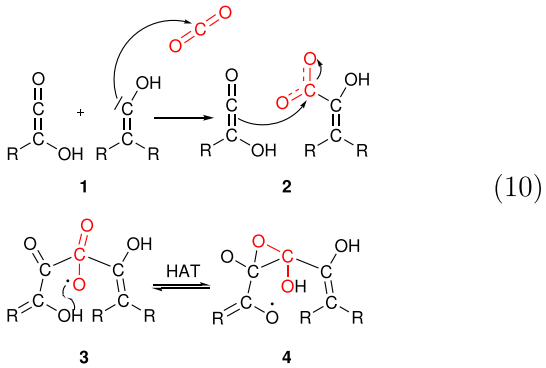

(10)

This step is rather strongly exergonic by −0.80 eV (Figure 8). As a part of this reaction, a hydrogen is transferred from an adjacent alcohol which in turn is oxidized to a ketone. In addition to this, the second C−O$^{\bullet}$ radical stabilizes itself by forming an epoxide with the adjacent carbon atom (reaction 10). Breaking the epoxide electrochemically is a well-established reaction[133,134] for which no major barriers are expected.

Overall, chain linkage proceeds through the CO_2 insertion between a ketene and a singly hydrogenated ketene. Contrary to the simple chain propagation, we see some evidence that CeO_2 contributes to the reaction more directly than just acting as an anchor. For example, it stabilizes reaction intermediates through hydrogen bonds or by allowing for hydrogen-atom transfers. The chain linkage requires a comparable onset potential as the general chain propagation reactions and is therefore energetically feasible if the initial propagation steps can occur.

Chain Branching. In addition to the linkage of chains, building connections between independently growing polymers is also a necessary requirement for the formation of carbonaceous materials or hard carbon. The linkage of independent chains or the formation of cyclopentadiene (5-membered unsaturated rings) or benzene rings (6-membered unsaturated rings) can also proceed through an equivalent electrochemical aldol condensation-type mechanism. The reaction is exemplified by considering the formation of a cyclopentadiene ring from a fully conjugated enol chain as a precursor (Figure 10). Attempts to form 6-membered rings failed owing to the very high tendency of ketenes for ring closure. However, numerous reactions for ring expansion which could increase the ring size from a 5-membered to a 6-membered ring are known in organic chemistry.[105,135] Furthermore, the restriction to a 5-membered ring is the result of the rather special reaction steps considered by us which assumes the simultaneous formation of side chains in early stages. For example, the linkage of longer side chains through formation of a carbene followed by insertion of CO_2 would directly result in the formation of a 6-membered ring. Studying all possible reactions is, however, highly complex and therefore far beyond the scope of this contribution.

Identical to the previously discussed steps, chain branching is also initialized by the elimination of one of the OH groups as water to form a carbene. This reaction can proceed through a purely chemical step which involves a hydrogen-atom transfer from one of the adjacent alcohol groups (CR-0 to CR-1 in Figure 10). This reaction is moderately exergonic by −0.4 eV (Figure 11). The surprisingly favorable energetics are a direct result of the possibility to delocalize the otherwise highly reactive free electron pair at the carbene through a long conjugated π-electron system and the newly formed ketone. Additionally, there is also a localized basin between the hydrogen of the adjacent alcohol and the carbene in the DORI (Figure 9). This indicates the presence of a strong hydrogen bond, which stabilizes the free electron pair further. In line with this, we also observe a rather short COH···C distance of 1.92 Å. Besides the chemical path, an electrochemical water elimination is also possible. This reaction is also energetically favorable and requires a positive potential of 0.1 V vs SHE.

Once the carbene has been formed, C−C bond formation is achieved through a nucleophilic attack at dissolved CO_2 (CR-2 to CR-3 in Figure 10). Assuming a direct attack without prior reduction of the newly formed keto group, this step is moderately exergonic by −0.4 eV (Figure 11). However, also the competing reduction of the newly formed ketone is thermodynamically highly favorable under experimental conditions since it occurs already at a rather positive potential of 0.2 V vs SHE (Figure 11). If this reduction takes place prior to the nucleophilic attack, then C−C bond formation becomes strongly exergonic by −1.8 eV (Figure 11).

C−C bond formation is followed by the reduction of the hydrogenation of the R−COO group to form a carbonic acid (R−COOH) and water elimination. The former step requires

https://doi.org/10.1021/acs.jpcc.3c08356
J. Phys. Chem. C XXXX, XXX, XXX−XXX

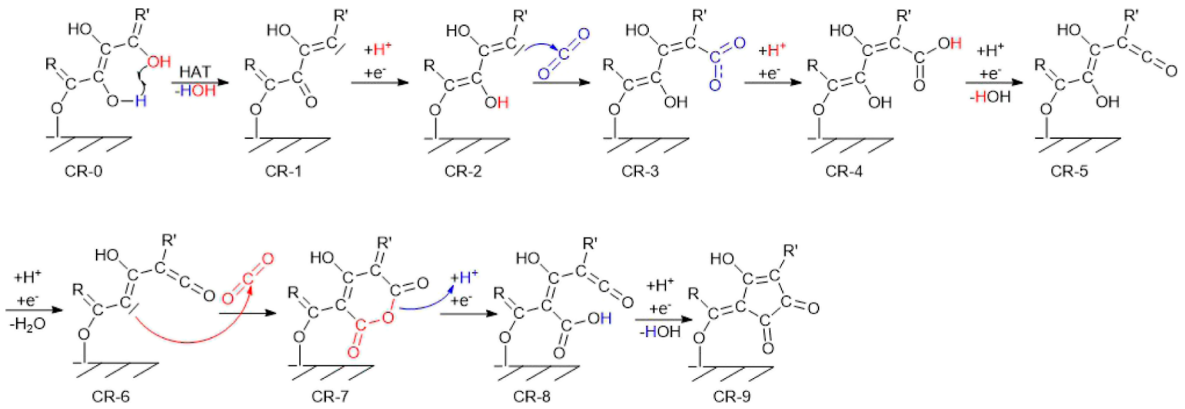

Figure 10. Summary of an example reaction mechanism for the formation of side chains.

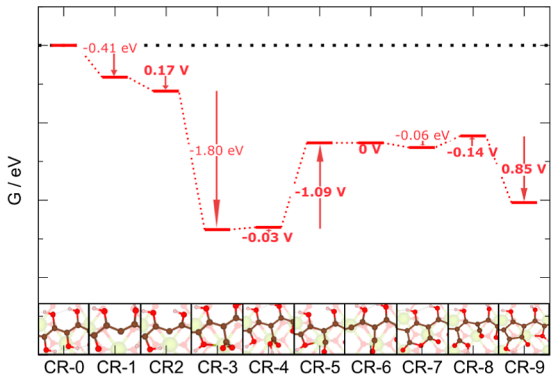

Figure 11. Energetics of the example mechanism for the branching of the olefin chain. Ce: lime, C: brown, O: red, and H: gray.

a potential of approximately 0.0 V vs SHE (CR-3 to CR-4 in Figure 11) which renders it thermodynamically favorable. The water elimination step to form a ketene on the other hand requires a much more negative potential of −1.1 V vs SHE which can still be overcome under CO_2RR conditions (CR-4 to CR-5 in Figure 11). Following the ketene formation, the side chain can grow, identical to the chain propagation mechanism, through an electrochemical aldol condensation (compare to Figure 4). Considering the repetitive nature of this polymerization mechanism, it is reasonable to assume that all subsequent steps require energies similar to the chain propagation steps (Figure 4).

An interesting side reaction is observed in the presence of an adjacent ketone. Here, water elimination does not lead to the formation of a ketene but rather results in the direct formation of an unsaturated γ-lactone (5-membered cyclic ester; reaction 11).

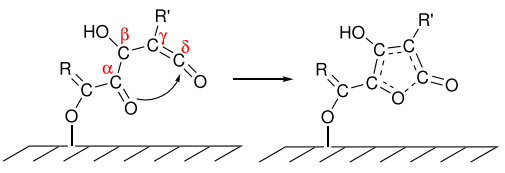

(11)

Thanks to the ester formation, this reaction is energetically highly favorable and occurs already at a very positive potential of 1.0 V vs SHE. The lactone can be split through a simple ester hydrolysis[106,136,137] and therefore does not constitute a dead end.

Naturally, a second chain can also start to grow in the vicinity through an additional elimination of an alcohol (CR-5 to CR-6 in Figure 10). Assuming an electrochemical water elimination step, this reaction occurs already at a potential of 0.0 V vs SHE. The subsequent C−C bond formation is then roughly thermoneutral (ΔG = −0.1 eV) and results in the direct formation of a glutaconic anhydride derivative (6-membered cyclic anhydride; CR-6 to CR-7 in Figure 10). This reaction is not unexpected considering that the formed carboxylate is a fair nucleophile and ketenes are highly susceptible to nucleophilic attacks.

The anhydride is easily split electrochemically at a potential of −0.1 V vs SHE. This results in the formation of a carbonic acid and a ketene (CR-7 to CR-8 in Figure 10). Eliminating the OH group of the carbonic acid finally initiates a concerted reaction step in which water is eliminated and a cyclopent-3-ene-1,2-dione derivative is formed (cyclic 5-membered ring with two keto groups; CR-8 to CR-9 in Figure 10). The overall reaction is energetically highly favorable and thus possible at the electrode potential applied in experiment.[52]

CONCLUSIONS

Inspired by well-established reactions in organic chemistry, we have evaluated the reaction mechanisms for CO_2 reduction over CeO_2(110). According to our computations, the reaction is initialized by the adsorption of CO_2 into an oxygen vacancy site. Owing to the rich defect chemistry of ceria, suitable sites are ample. This renders the initial CO_2 adsorption step feasible despite being endergonic. C−C bond formation is then achieved through an Eley−Rideal-type aldol condensation in which a carbene intermediate performs a nucleophilic attack on CO_2. This is followed by the formation of a new carbene through the electrochemical elimination of water. Interestingly, only the initial adsorption step is strongly affected by ceria, while all other steps appear to be almost completely independent from the catalyst. This mechanism is completely generic and can be repeated for all steps of the polymerization of CO_2. This fundamental mechanistic understanding lays the foundation for the development of enhanced catalysts for the conversion of CO_2 to hard carbon and may also help to develop new routes for the electrosynthesis of organic compounds.

https://doi.org/10.1021/acs.jpcc.3c08356
J. Phys. Chem. C XXXX, XXX, XXX−XXX

■ ASSOCIATED CONTENT

Supporting Information

The Supporting Information is available free of charge at https://pubs.acs.org/doi/10.1021/acs.jpcc.3c08356.

Justification for use of the DFT method, description of computation of the Pourbaix diagram, vacancy formation energies, important Bader charges, summary of all considered reaction mechanisms, and selected density of states (PDF)

■ AUTHOR INFORMATION

Corresponding Author

Michael Busch − *Institute of Theoretical Chemistry, Ulm University, 89081 Ulm, Germany; Division of Materials Science, Department of Engineering Sciences and Mathematics and Wallenberg Initiative Materials Science for Sustainability (WISE), Luleå University of Technology, 971 87 Luleå, Sweden;* orcid.org/0000-0003-0223-2772; Email: michael.busch@ltu.se

Authors

Florian Keller − *Institute of Theoretical Chemistry, Ulm University, 89081 Ulm, Germany;* Present Address: Institut für Chemie (IFC), University of Zurich, Winterthurerstrasse 190, 8057 Zürich, Switzerland

Johannes Döhn − *Institute of Theoretical Chemistry, Ulm University, 89081 Ulm, Germany*

Axel Groß − *Institute of Theoretical Chemistry, Ulm University, 89081 Ulm, Germany;* orcid.org/0000-0003-4037-7331

Complete contact information is available at: https://pubs.acs.org/10.1021/acs.jpcc.3c08356

Notes

The authors declare no competing financial interest.

■ ACKNOWLEDGMENTS

F.K. and J.D. acknowledge funding through the German Bundesministerium für Bildung und Forschung (BMBF) project NETPEC (grant number: 01LS2103A). M.B. is grateful for financial support from the Dr. Barbara-Mez-Starck foundation. Computer time provided by the state of Baden-Württemberg through bwHPC and the German Research Foundation (DFG) through grant no INST 40/575-1 FUGG (JUSTUS 2 cluster) is gratefully acknowledged.

■ REFERENCES

(1) Friedlingstein, P.; O'Sullivan, M.; Jones, M. W.; Andrew, R. M.; Gregor, L.; Hauck, J.; Le Quéré, C.; Luijkx, I. T.; Olsen, A.; Peters, G. P.; et al. Global Carbon Budget 2022. *Earth Syst. Sci. Data* **2022**, *14*, 4811−4900.

(2) Lüthi, D.; Le Floch, M.; Bereiter, B.; Blunier, T.; Barnola, J.-M.; Siegenthaler, U.; Raynaud, D.; Jouzel, J.; Fischer, H.; Kawamura, K.; et al. High-resolution carbon dioxide concentration record 650,000−800,000 years before present. *Nature* **2008**, *453*, 379−382.

(3) Rau, G. H. The race to remove CO2 needs more contestants. *Nat. Clim. Change* **2019**, *9*, 256.

(4) May, M. M.; Rehfeld, K. Negative Emissions as the New Frontier of Photoelectrochemical CO_2 Reduction. *Adv. Energy Mater.* **2022**, *12*, 2103801.

(5) Erşan, S.; Park, J. O. Light-Independent Biological Conversion of CO2. *Joule* **2020**, *4*, 2047−2051.

(6) Onyeaka, H.; Miri, T.; Obileke, K.; Hart, A.; Anumudu, C.; Al-Sharify, Z. T. Minimizing carbon footprint via microalgae as a biological capture. *Carbon Capture Sci. Technol.* **2021**, *1*, 100007.

(7) Gabrielli, P.; Gazzani, M.; Mazzotti, M. The Role of Carbon Capture and Utilization, Carbon Capture and Storage, and Biomass to Enable a Net-Zero-CO_2 Emissions Chemical Industry. *Ind. Eng. Chem. Res.* **2020**, *59*, 7033−7045.

(8) Lefebvre, D.; Williams, A. G.; Kirk, G. J. D.; Paul; Burgess, J.; Meersmans, J.; Silman, M. R.; Román-Dañobeytia, F.; Farfan, J.; Smith, P. Assessing the carbon capture potential of a reforestation project. *Sci. Rep.* **2021**, *11*, 19907.

(9) Kelemen, P.; Benson, S. M.; Pilorgé, H.; Psarras, P.; Wilcox, J. An Overview of the Status and Challenges of CO2 Storage in Minerals and Geological Formations. *Front. Clim.* **2019**, *1*, 9.

(10) Saha, P.; Amanullah, S.; Dey, A. Selectivity in Electrochemical CO_2 Reduction. *Acc. Chem. Res.* **2022**, *55*, 134−144.

(11) Shafaat, H. S.; Yang, J. Y. Uniting biological and chemical strategies for selective CO2 reduction. *Nat. Catal.* **2021**, *4*, 928−933.

(12) Overa, S.; Ko, B. H.; Zhao, Y.; Jiao, F. Electrochemical Approaches for CO_2 Conversion to Chemicals: A Journey toward Practical Applications. *Acc. Chem. Res.* **2022**, *55*, 638−648.

(13) May, M. M.; Rehfeld, K. ESD Ideas: Photoelectrochemical carbon removal as negative emission technology. *Earth Syst. Dyn.* **2019**, *10*, 1−7.

(14) Paris, A. R.; Bocarsly, A. B. High-Efficiency Conversion of CO_2 to Oxalate in Water Is Possible Using a Cr-Ga Oxide Electrocatalyst. *ACS Catal.* **2019**, *9*, 2324−2333.

(15) Schuler, E.; Demetriou, M.; Shiju, N. R.; Gruter, G.-J. M. Towards Sustainable Oxalic Acid from CO_2 and Biomass. *ChemSusChem* **2021**, *14*, 3636−3664.

(16) Ren, J.; Li, F.-F.; Lau, J.; González-Urbina, L.; Licht, S. One-Pot Synthesis of Carbon Nanofibers from CO. *Nano Lett.* **2015**, *15*, 6142−6148.

(17) Pastero, L.; Curetti, N.; Ortenzi, M. A.; Schiavoni, M.; Destefanis, E.; Pavese, A. CO2 capture and sequestration in stable Ca-oxalate, via Ca-ascorbate promoted green reaction. *Sci. Total Environ.* **2019**, *666*, 1232−1244.

(18) Angamuthu, R.; Byers, P.; Lutz, M.; Spek, A. L.; Bouwman, E. Electrocatalytic CO_2 Conversion to Oxalate by a Copper Complex. *Science* **2010**, *327*, 313−315.

(19) García de Arquer, F. P.; Dinh, C.-T.; Ozden, A.; Wicks, J.; McCallum, C.; Kirmani, A. R.; Nam, D.-H.; Gabardo, C.; Seifitokaldani, A.; Wang, X.; et al. CO_2 electrolysis to multicarbon products at activities greater than 1 Acm-2. *Science* **2020**, *367*, 661−666.

(20) Ritchie, H.; Roser, M.; Rosado, P. *CO_2 and Greenhouse Gas Emissions. Our World in Data*, 2020. https://ourworldindata.org/co2-and-greenhouse-gas-emissions.

(21) MacDowell, N.; Florin, N.; Buchard, A.; Hallett, J.; Galindo, A.; Jackson, G.; Adjiman, C. S.; Williams, C. K.; Shah, N.; Fennell, P. An overview of CO2 capture technologies. *Energy Environ. Sci.* **2010**, *3*, 1645.

(22) Bouzalakos, S.; Mercedes, M. *Developments and Innovation in Carbon Dioxide (CO2) Capture and Storage Technology*; Elsevier, 2010; pp 1−24.

(23) Melián-Cabrera, I.; Granados, M. L.; Fierro, J. *Catal. Lett.* **2002**, *79*, 165−170.

(24) Melián-Cabrera, I.; López Granados, M.; Fierro, J. Reverse Topotactic Transformation of a Cu−Zn−Al Catalyst during Wet Pd Impregnation: Relevance for the Performance in Methanol Synthesis from CO2/H2Mixtures. *J. Catal.* **2002**, *210*, 273−284.

(25) Bowker, M. Methanol Synthesis from CO_2 Hydrogenation. *ChemCatChem* **2019**, *11*, 4238−4246.

(26) Posada-Borbón, A.; Grönbeck, H. A First-Principles-Based Microkinetic Study of CO_2 Reduction to CH_3OH over In_2O_3(110). *ACS Catal.* **2021**, *11*, 9996−10006.

(27) Francke, R.; Schille, B.; Roemelt, M. Homogeneously Catalyzed Electroreduction of Carbon Dioxide—Methods, Mechanisms, and Catalysts. *Chem. Rev.* **2018**, *118*, 4631−4701.

(28) Rakowski Dubois, M.; Dubois, D. L. Development of Molecular Electrocatalysts for CO_2 Reduction and H_2 Production/Oxidation. *Acc. Chem. Res.* **2009**, *42*, 1974−1982.
(29) Hawecker, J.; Lehn, J.-M.; Ziessel, R. Electrocatalytic reduction of carbon dioxide mediated by Re(bipy)$(CO)_3$Cl (bipy = 2,2′-bipyridine). *J. Chem. Soc., Chem. Commun.* **1984**, 328−330.
(30) Sullivan, B. P.; Bolinger, C. M.; Conrad, D.; Vining, W. J.; Meyer, T. J. One- and two-electron pathways in the electrocatalytic reduction of CO_2 by fac-Re(bpy)$(CO)_3$Cl (bpy = 2,2′-bipyridine). *J. Chem. Soc., Chem. Commun.* **1985**, 1414−1416.
(31) Zhang, S.; Fan, Q.; Xia, R.; Meyer, T. J. CO_2 Reduction: From Homogeneous to Heterogeneous Electrocatalysis. *Acc. Chem. Res.* **2020**, *53*, 255−264.
(32) Zhang, S.; Kang, P.; Bakir, M.; Lapides, A. M.; Dares, C. J.; Meyer, T. J. Polymer-supported CuPd nanoalloy as a synergistic catalyst for electrocatalytic reduction of carbon dioxide to methane. *Proc. Natl. Acad. Sci. U.S.A.* **2015**, *112* (52), 15809−15814.
(33) Wang, Y.; Wang, D.; Dares, C. J.; Marquard, S. L.; Sheridan, M. V.; Meyer, T. J. CO_2 reduction to acetate in mixtures of ultrasmall $(Cu)_n(Ag)_m$ bimetallic nanoparticles. *Proc. Natl. Acad. Sci. U.S.A.* **2017**, *115* (2), 278−283.
(34) Kaneco, S.; Katsumata, H.; Suzuki, T.; Ohta, K. Electrochemical reduction of carbon dioxide to ethylene at a copper electrode in methanol using potassium hydroxide and rubidium hydroxide supporting electrolytes. *Electrochim. Acta* **2006**, *51*, 3316−3321.
(35) Cometto, C.; Chen, L.; Lo, P.; Guo, Z.; Lau, K.; Anxolabehere-Mallart, E.; Fave, C.; Lau, T.; Robert, M. Highly Selective Molecular Catalysts for the CO2-to-CO Electrochemical Conversion at Very Low Overpotential. Contrasting Fe vs Co Quaterpyridine Complexes upon Mechanistic Studies. *ACS Catal.* **2018**, *8*, 3411−3417.
(36) Cometto, C.; Chen, L.; Mendoza, D.; Lassalle-Kaiser, B.; Lau, T.; Robert, M. An Iron Quaterpyridine Complex as Precursor for the Electrocatalytic Reduction of CO2 to Methane. *ChemSusChem* **2019**, *12*, 4500−4505.
(37) Costentin, C.; Drouet, S.; Robert, M.; Savéant, J. M. A Local Proton Source Enhances CO2 Electroreduction to CO by a Molecular Fe Catalyst. *Science* **2012**, *338*, 90−94.
(38) Shen, J.; Kortlever, R.; Kas, R.; Birdja, Y.; Diaz-Morales, O.; Kwon, Y.; Ledezma-Yanez, I.; Schouten, K.; Mul, G.; Koper, M. Electrocatalytic reduction of carbon dioxide to carbon monoxide and methane at an immobilized cobalt protoporphyrin. *Nature Commun.* **2015**, *6*, 8177.
(39) Khakpour, R.; Lindberg, D.; Laasonen, K.; Busch, M. CO_2 or Carbonates − What is the Active Species in Electrochemical CO_2 Reduction over Fe-Porphyrin? *ChemCatChem* **2023**, *15*, No. e2022016.
(40) Khakpour, R.; Laasonen, K.; Busch, M. Selectivity of CO2, carbonic acid and bicarbonate electroreduction over Iron-porphyrin catalyst: A DFT study. *Electrochim. Acta* **2023**, *442*, 141784.
(41) Göttle, A. J.; Koper, M. Determinant Role of Electrogenerated Reactive Nucleophilic Species on Selectivity during Reduction of CO2 Catalyzed by Metalloporphyrins. *J. Am. Chem. Soc.* **2018**, *140*, 4826−4834.
(42) Hossain, M. N.; Khakpour, R.; Busch, M.; Suominen, M.; Laasonen, K.; Kallio, T. Temperature-Controlled Syngas Production via Electrochemical CO_2 Reduction on a CoTPP/MWCNT Composite in a Flow Cell. *ACS Appl. Energy Mater.* **2022**, *6* (1), 267−277.
(43) Dong, S.-T.; Xu, C.; Lassalle-Kaiser, B. Multiple C−C bond formation upon electrocatalytic reduction of CO2 by an iron-based molecular macrocycle. *Chem. Sci.* **2023**, *14*, 550−556.
(44) Boutin, E.; Wang, M.; Lin, J.; Mesnage, M.; Mendoza, D.; Lassalle-Kaiser, B.; Hahn, C.; Jaramillo, T.; Robert, M. Aqueous Electrochemical Reduction of Carbon Dioxide and Carbon Monoxide into Methanol with Cobalt Phthalocyanine. *Angew. Chem., Int. Ed.* **2019**, *58*, 16172−16176.
(45) Varela, A.; Ranjbar Sahraie, N.; Steinberg, J.; Ju, W.; Oh, H.; Strasser, P. Metal-Doped Nitrogenated Carbon as an Efficient Catalyst for Direct CO2 Electroreduction to CO and Hydrocarbons. *Angew. Chem., Int. Ed.* **2015**, *54*, 10758−10762.
(46) Ju, W.; Bagger, A.; Wang, X.; Tsai, Y.; Luo, F.; Möller, T.; Wang, H.; Rossmeisl, J.; Varela, A.; Strasser, P. Unraveling Mechanistic Reaction Pathways of the Electrochemical CO2 Reduction on Fe−N−C Single-Site Catalysts. *ACS Energy Lett.* **2019**, *4*, 1663−1671.
(47) Nitopi, S.; Bertheussen, E.; Scott, S.; Liu, X.; Engstfeld, A.; Horch, S.; Seger, B.; Stephens, I.; Chan, K.; Hahn, C.; et al. Progress and Perspectives of Electrochemical CO2 Reduction on Copper in Aqueous Electrolyte. *Chem. Rev.* **2019**, *119*, 7610−7672.
(48) Mangione, G.; Huang, J.; Buonsanti, R.; Corminboeuf, C. Dual-Facet Mechanism in Copper Nanocubes for Electrochemical CO2 Reduction into Ethylene. *J. Phys. Chem. Lett.* **2019**, *10*, 4259−4265.
(49) Ikeda, S.; Takagi, T.; Ito, K. Selective Formation of Formic Acid, Oxalic Acid, and Carbon Monoxide by Electrochemical Reduction of Carbon Dioxide. *Bull. Chem. Soc. Jpn.* **1987**, *60*, 2517−2522.
(50) Fischer, J.; Lehmann, T.; Heitz, E. The production of oxalic acid from CO2 and H2O. *J. Appl. Electrochem.* **1981**, *11*, 743−750.
(51) Marx, M.; Frauendorf, H.; Spannenberg, A.; Neumann, H.; Beller, M. Revisiting Reduction of CO_2 to Oxalate with First-Row Transition Metals: Irreproducibility, Ambiguous Analysis, and Conflicting Reactivity. *JACS Au* **2022**, *2*, 731−744.
(52) Esrafilzadeh, D.; Zavabeti, A.; Jalili, R.; Atkin, P.; Choi, J.; Carey, B. J.; Brkljača, R.; O'Mullane, A. P.; Dickey, M. D.; Officer, D. L.; et al. Room temperature CO2 reduction to solid carbon species on liquid metals featuring atomically thin ceria interfaces. *Nat. Commun.* **2019**, *10*, 865.
(53) Liu, S.; Wu, X.; Weng, D.; Ran, R. Ceria-based catalysts for soot oxidation: a review. *J. Rare Earths* **2015**, *33*, 567−590.
(54) LeValley, T. L.; Richard, A. R.; Fan, M. The progress in water gas shift and steam reforming hydrogen production technologies - A review. *Int. J. Hydrogen Energy* **2014**, *39*, 16983−17000.
(55) Symington, A. R.; Harker, R. M.; Storr, M. T.; Molinari, M.; Parker, S. C. Thermodynamic Evolution of Cerium Oxide Nanoparticle Morphology Using Carbon Dioxide. *J. Phys. Chem. C* **2020**, *124*, 23210−23220.
(56) Perdew, J. P.; Burke, K.; Ernzerhof, M. Generalized Gradient Approximation Made Simple. *Phys. Rev. Lett.* **1996**, *77*, 3865−3868.
(57) Grimme, S. Semiempirical GGA-type density functional constructed with a long-range dispersion correction. *J. Comput. Chem.* **2006**, *27*, 1787−1799.
(58) Grimme, S.; Antony, J.; Ehrlich, S.; Krieg, H. A consistent and accurate ab-initio parametrization of density functional dispersion correction (DFT-D) for the 94 elements H-Pu. *J. Chem. Phys.* **2010**, *132*, 154104.
(59) Grimme, S.; Ehrlich, S.; Goerigk, L. Effect of the damping function in dispersion corrected density functional theory. *J. Comput. Chem.* **2011**, *32*, 1456−1465.
(60) Kresse, G.; Joubert, D. From ultrasoft pseudopotentials to the projector augmented-wave method. *Phys. Rev. B* **1999**, *59*, 1758−1775.
(61) Dudarev, S. L.; Liechtenstein, A. I.; Castell, M. R.; Briggs, G. A. D.; Sutton, A. P. Surface states on NiO (100) and the origin of the contrast reversal in atomically resolved scanning tunneling microscope images. *Phys. Rev. B* **1997**, *56*, 4900−4908.
(62) Dudarev, S. L.; Botton, G. A.; Savrasov, S. Y.; Humphreys, C. J.; Sutton, A. P. Electron-energy-loss spectra and the structural stability of nickel oxide: An LSDA+U study. *Phys. Rev. B* **1998**, *57*, 1505−1509.
(63) Paier, J.; Penschke, C.; Sauer, J. Oxygen Defects and Surface Chemistry of Ceria: Quantum Chemical Studies Compared to Experiment. *Chem. Rev.* **2013**, *113*, 3949−3985.
(64) Blöchl, P. E.; Jepsen, O.; Andersen, O. K. Improved tetrahedron method for Brillouin-zone integrations. *Phys. Rev. B* **1994**, *49*, 16223−16233.

https://doi.org/10.1021/acs.jpcc.3c08356
J. Phys. Chem. C XXXX, XXX, XXX−XXX

(65) Chan, K.; Tsai, C.; Hansen, H. A.; Nørskov, J. K. Molybdenum Sulfides and Selenides as Possible Electrocatalysts for CO_2 Reduction. *ChemCatChem* **2014**, *6*, 1899−1905.
(66) Nørskov, J. K.; Rossmeisl, J.; Logadottir, A.; Lindqvist, L.; Kitchin, J. R.; Bligaard, T.; Jónsson, H. Origin of the Overpotential for Oxygen Reduction at a Fuel-Cell Cathode. *J. Phys. Chem. B* **2004**, *108*, 17886−17892.
(67) Mathew, K.; Kolluru, V. S. C.; Hennig, R. G. *VASPsol: Implicit solvation and electrolyte model for density-functional theory*, 2018. https://github.com/henniggroup/VASPsol.
(68) Mathew, K.; Sundararaman, R.; Letchworth-Weaver, K.; Arias, T. A.; Hennig, R. G. Implicit solvation model for density-functional study of nanocrystal surfaces and reaction pathways. *J. Chem. Phys.* **2014**, *140*, 084106.
(69) Mathew, K.; Kolluru, V. S. C.; Mula, S.; Steinmann, S. N.; Hennig, R. G. Implicit self-consistent electrolyte model in plane-wave density-functional theory. *J. Chem. Phys.* **2019**, *151*, 234101.
(70) GitHub Inc. *VASPsol convergence issue for CeO2(111)*, 2018. https://github.com/henniggroup/VASPsol/issues/36.
(71) Dupont, C.; Andreussi, O.; Marzari, N. Self-consistent continuum solvation (SCCS): The case of charged systems. *J. Chem. Phys.* **2013**, *139*, 214110.
(72) Kühne, T. D.; Iannuzzi, M.; Del Ben, M.; Rybkin, V. V.; Seewald, P.; Stein, F.; Laino, T.; Khaliullin, R. Z.; Schütt, O.; Schiffmann, F.; et al. CP2K: An electronic structure and molecular dynamics software package - Quickstep: Efficient and accurate electronic structure calculations. *J. Chem. Phys.* **2020**, *152*, 194103.
(73) Sundararaman, R.; Goddard, W. A. The charge-asymmetric nonlocally determined local-electric (CANDLE) solvation model. *J. Chem. Phys.* **2015**, *142*, 064107.
(74) Andreussi, O.; Dabo, I.; Marzari, N. Revised self-consistent continuum solvation in electronic-structure calculations. *J. Chem. Phys.* **2012**, *136*, 064102.
(75) Gunceler, D.; Letchworth-Weaver, K.; Sundararaman, R.; Schwarz, K. A.; Arias, T. A. The importance of nonlinear fluid response in joint density-functional theory studies of battery systems. *Modell. Simul. Mater. Sci. Eng.* **2013**, *21*, 074005.
(76) Sundararaman, R.; Letchworth-Weaver, K.; Schwarz, K. A.; Gunceler, D.; Ozhabes, Y.; Arias, T. JDFTx: Software for joint density-functional theory. *SoftwareX* **2017**, *6*, 278−284.
(77) Lundin, A.; Panas, I.; Ahlberg, E. Quantum Chemical Modeling of Ethene Epoxidation with Hydrogen Peroxide: The Effect of Microsolvation with Water. *J. Phys. Chem. A* **2007**, *111*, 9080−9086.
(78) Groß, A.; Sakong, S. Ab Initio Simulations of Water/Metal Interfaces. *Chem. Rev.* **2022**, *122*, 10746−10776.
(79) Busch, M.; Wang, R.; Hellman, A.; Rossmeisl, J.; Grönbeck, H. The Influence of Inert Ions on the Reactivity of Manganese Oxides. *J. Phys. Chem. C* **2018**, *122*, 216−226.
(80) Siahrostami, S.; Verdaguer-Casadevall, A.; Karamad, M.; Deiana, D.; Malacrida, P.; Wickman, B.; Escudero-Escribano, M.; Paoli, E.; Frydendal, R.; Hansen, T.; et al. Enabling direct H2O2 production through rational electrocatalyst design. *Nat. Mater.* **2013**, *12*, 1137−1143.
(81) Ju, W.; Bagger, A.; Hao, G.; Varela, A.; Sinev, I.; Bon, V.; Roldan Cuenya, B.; Kaskel, S.; Rossmeisl, J.; Strasser, P. Understanding activity and selectivity of metal-nitrogen-doped carbon catalysts for electrochemical reduction of CO2. *Nature Commun.* **2017**, *8*, 944.
(82) Song, F.; Busch, M.; Lassalle-Kaiser, B.; Hsu, C.; Petkucheva, E.; Bensimon, M.; Chen, H.; Corminboeuf, C.; Hu, X. An Unconventional Iron Nickel Catalyst for the Oxygen Evolution Reaction. *ACS Cent. Sci.* **2019**, *5*, 558−568.
(83) Groß, A. Grand-canonical approaches to understand structures and processes at electrochemical interfaces from an atomistic perspective. *Curr. Opin. Electrochem.* **2021**, *27*, 100684.
(84) Groß, A. Reversible vs Standard Hydrogen Electrode Scale in Interfacial Electrochemistry from a Theoretician's Atomistic Point of View. *J. Phys. Chem. C* **2022**, *126*, 11439−11446.
(85) Alongi, K.; Shields, G. Theoretical Calculations of Acid Dissociation Constants: A Review Article. *Annu. Rep. Comput. Chem.* **2010**, *6*, 113−138.
(86) Ho, J. Predicting pKa in Implicit Solvents: Current Status and Future Directions. *Aust. J. Chem.* **2014**, *67*, 1441−1460.
(87) Busch, M.; Ahlberg, E.; Ahlberg, E.; Laasonen, K. How to Predict the pKa of Any Compound in Any Solvent. *ACS Omega* **2022**, *7*, 17369−17383.
(88) Busch, M.; Ahlberg, E.; Laasonen, K. From absolute potentials to a generalized computational standard hydrogen electrode for aqueous and non-aqueous solvents. *Phys. Chem. Chem. Phys.* **2021**, *23*, 11727−11737.
(89) Lide, D. R. *CRC Handbook of Chemistry and Physic*; CRC Press Inc; 84th ed., 2003.
(90) Frisch, M. e.; Trucks, G.; Schlegel, H.; Scuseria, G.; Robb, M.; Cheeseman, J.; Scalmani, G.; Barone, V.; Petersson, G.; Nakatsuji, H.; et al. *Gaussian 16*, 2016.
(91) Zhao, Y.; Truhlar, D. G. The M06 suite of density functionals for main group thermochemistry, thermochemical kinetics, noncovalent interactions, excited states, and transition elements: two new functionals and systematic testing of four M06-class functionals and 12 other functionals. *Theor. Chem. Acc.* **2008**, *120*, 215−241.
(92) Marenich, A. V.; Cramer, C. J.; Truhlar, D. G. Universal Solvation Model Based on Solute Electron Density and on a Continuum Model of the Solvent Defined by the Bulk Dielectric Constant and Atomic Surface Tensions. *J. Phys. Chem. B* **2009**, *113*, 6378−−6396.
(93) Etim, U. J.; Zhang, C.; Zhong, Z. Impacts of the Catalyst Structures on CO2 Activation on Catalyst Surfaces. *Nanomaterials* **2021**, *11*, 3265.
(94) Li, H.; Zhao, J.; Luo, L.; Du, J.; Zeng, J. Symmetry-Breaking Sites for Activating Linear Carbon Dioxide Molecules. *Acc. Chem. Res.* **2021**, *54*, 1454−1464.
(95) Hollemannn, A. F.; Wiberg, N. *Anorganische Chemie*, 102nd ed.; Walter de Gruyter: Berlin, 2007.
(96) Busch, M.; Ahlberg, E.; Laasonen, K. Universal Trends between Acid Dissociation Constants in Protic and Aprotic Solvents. *Chem.—Eur. J.* **2022**, *28*, No. e202201667.
(97) Channei, D.; Phanichphant, S.; Nakaruk, A.; Mofarah, S.; Koshy, P.; Sorrell, C. Aqueous and Surface Chemistries of Photocatalytic Fe-Doped CeO2 Nanoparticles. *Catalysts* **2017**, *7*, 45.
(98) Ma, Y.; Ma, Y.; Giuli, G.; Euchner, H.; Groß, A.; Lepore, G. O.; d'Acapito, F.; Geiger, D.; Biskupek, J.; Kaiser, U.; et al. Introducing Highly Redox-Active Atomic Centers into Insertion-Type Electrodes for Lithium-Ion Batteries. *Adv. Energy Mater.* **2020**, *10*, 2000783.
(99) Sayle, T. X. T.; Parker, S. C.; Sayle, D. C. Shape of CeO2 nanoparticles using simulated amorphisation and recrystallisation. *Chem. Commun.* **2004**, *2438*, 2438.
(100) Fronzi, M.; Soon, A.; Delley, B.; Traversa, E.; Stampfl, C. Stability and morphology of cerium oxide surfaces in an oxidizing environment: A first-principles investigation. *J. Chem. Phys.* **2009**, *131*, 104701.
(101) Skorodumova, N. V.; Baudin, M.; Hermansson, K. Surface properties of CeO2 from first principles. *Phys. Rev. B* **2004**, *69*, 075401.
(102) Nolan, M.; Parker, S. C.; Watson, G. W. The electronic structure of oxygen vacancy defects at the low index surfaces of ceria. *Surf. Sci.* **2005**, *595*, 223−232.
(103) Scanlon, D. O.; Galea, N. M.; Morgan, B. J.; Watson, G. W. Reactivity on the (110) Surface of Ceria: A GGA+U Study of Surface Reduction and the Adsorption of CO and NO_2. *J. Phys. Chem. C* **2009**, *113*, 11095−11103.
(104) Song, Y.-L.; Yin, L.-L.; Zhang, J.; Hu, P.; Gong, X.-Q.; Lu, G. A DFT+U study of CO oxidation at CeO2(110) and (111) surfaces with oxygen vacancies. *Surf. Sci.* **2013**, *618* (618), 140−147.
(105) Bruckner, R. *Reaktionsmechanismen*, 2nd ed.; Spektrum Akademischer Verlag, 2002.

https://doi.org/10.1021/acs.jpcc.3c08356
J. Phys. Chem. C XXXX, XXX, XXX−XXX

(106) Vollhardt, K. P. C.; Schore, N. E. *Organische Chemie*, 5th ed.; Butenschon, H., Ed.; *Wiley-VCH-Lehrbuchkollektion 1*; Wiley-VCH Verlag: Weinheim, Germany, 2011.
(107) Heck, R. F.; Nolley, J. P. Palladium-catalyzed vinylic hydrogen substitution reactions with aryl, benzyl, and styryl halides. *J. Org. Chem.* **1972**, *37*, 2320−2322.
(108) Wurtz, A. Ueber eine neue Klasse organischer Radicale. *Ann. Chem. Pharm.* **1855**, *96*, 364−375.
(109) Yoshikawa, K.; Kaneeda, M.; Nakamura, H. Development of Novel CeO2-based CO2 adsorbent and analysis on its CO2 adsorption and desorption mechanism. *Energy Procedia* **2017**, *114*, 2481−2487.
(110) Baumann, N.; Lan, J.; Iannuzzi, M. CO2 adsorption on the pristine and reduced CeO2 (111) surface: Geometries and vibrational spectra by first principles simulations. *J. Chem. Phys.* **2021**, *154*, 094702.
(111) Wang, M.; Shen, M.; Jin, X.; Tian, J.; Zhou, Y.; Shao, Y.; Zhang, L.; Li, Y.; Shi, J. Mild generation of surface oxygen vacancies on CeO_2 for improved CO_2 photoreduction activity. *Nanoscale* **2020**, *12*, 12374−12382.
(112) Elschenbroich, C.; Salzer, A. *Organometallics*, 2nd ed.; *Organometallics*; Wiley-VCH Verlag: Weinheim, Germany, 1992.
(113) Visibile, A.; Wang, R. B.; Vertova, A.; Rondinini, S.; Minguzzi, A.; Ahlberg, E.; Busch, M. Influence of Strain on the Band Gap of Cu_2O. *Chem. Mater.* **2019**, *31*, 4787−4792.
(114) Sakong, S.; Mahlberg, D.; Roman, T.; Li, M.; Pandey, M.; Groß, A. Influence of Local Inhomogeneities and the Electrochemical Environment on the Oxygen Reduction Reaction on Pt-Based Electrodes: A DFT Study. *J. Phys. Chem. C* **2020**, *124*, 27604−27613.
(115) Busch, M.; Halck, N. B.; Kramm, U. I.; Siahrostami, S.; Krtil, P.; Rossmeisl, J. Beyond the top of the volcano? − A unified approach to electrocatalytic oxygen reduction and oxygen evolution. *Nano Energy* **2016**, *29*, 126−135.
(116) Alvarado-Ávila, M. I.; Toledo-Carrillo, E.; Dutta, J. Cerium Oxide on a Fluorinated Carbon-Based Electrode as a Promising Catalyst for Hypochlorite Production. *ACS Omega* **2022**, *7*, 37465−37475.
(117) McCrory, C.; Jung, S.; Peters, J.; Jaramillo, T. Benchmarking Heterogeneous Electrocatalysts for the Oxygen Evolution Reaction. *J. Am. Chem. Soc.* **2013**, *135*, 16977−16987.
(118) McCrory, C.; Jung, S.; Ferrer, I.; Chatman, S.; Peters, J.; Jaramillo, T. Benchmarking Hydrogen Evolving Reaction and Oxygen Evolving Reaction Electrocatalysts for Solar Water Splitting Devices. *J. Am. Chem. Soc.* **2015**, *137*, 4347−4357.
(119) Roger, I.; Symes, M. Silver Leakage from Ag/AgCl Reference Electrodes as a Potential Cause of Interference in the Electrocatalytic Hydrogen Evolution Reaction. *ACS Appl. Mater. Interfaces* **2017**, *9*, 472−478.
(120) Frydendal, R.; Busch, M.; Halck, N.; Paoli, E.; Krtil, P.; Chorkendorff, I.; Rossmeisl, J. Enhancing Activity for the Oxygen Evolution Reaction: The Beneficial Interaction of Gold with Manganese and Cobalt Oxides. *ChemCatChem* **2015**, *7*, 149−154.
(121) Gorlin, Y.; Chung, C.; Benck, J.; Nordlund, D.; Seitz, L.; Weng, T.; Sokaras, D.; Clemens, B.; Jaramillo, T. Understanding Interactions between Manganese Oxide and Gold That Lead to Enhanced Activity for Electrocatalytic Water Oxidation. *J. Am. Chem. Soc.* **2014**, *136*, 4920−4926.
(122) Khakpour, R.; Farshadfar, K.; Dong, S.; Lassalle-Kaiser, B.; Laasonen, K.; Busch, M. *J. Phys. Chem. C* **2024**, DOI: 10.1021/acs.jpcc.3c08347.
(123) Blyholder, G. Molecular Orbital View of Chemisorbed Carbon Monoxide. *J. Phys. Chem.* **1964**, *68*, 2772−2777.
(124) Staudinger, H. Zur Kenntniss der Ketene. Diphenylketen. *Justus Liebigs Ann. Chem.* **1907**, *356*, 51−123.
(125) Heenen, H. H.; Shin, H.; Kastlunger, G.; Overa, S.; Gauthier, J. A.; Jiao, F.; Chan, K. The mechanism for acetate formation in electrochemical CO(2) reduction on Cu: selectivity with potential, pH, and nanostructuring. *Energy Environ. Sci.* **2022**, *15*, 3978−3990.
(126) Seidl, E. T.; Schaefer, H. F. I. I. I. Theoretical investigation of the dimerization of ketene: does the 2S + 2A cycloaddition reaction exist? *J. Am. Chem. Soc.* **1991**, *113*, 5195−5200.
(127) Huisgen, R.; Otto, P. The mechanism of dimerization of dimethylketene. *J. Am. Chem. Soc.* **1968**, *90*, 5342−5343.
(128) Staudinger, H. Ketene, eine neue Körperklasse. *Ber. Dtsch. Chem. Ges.* **1905**, *38*, 1735−1739.
(129) Wedekind, E. Ueber die Gewinnung von Säureanhydriden mit Hülfe von tertiären Aminen. *Ber. Dtsch. Chem. Ges.* **1901**, *34*, 2070−2077.
(130) Wedeking, E.; Weisswange, W. Ueber die Synthese eines Diketons der Cyclobutanreihe. *Ber. Dtsch. Chem. Ges.* **1906**, *39*, 1631−1646.
(131) Wedekind, E. Ueber das Verhalten einiger Säurechloride bei der Chlorwasserstoffentziehung. *Justus Liebigs Ann. Chem.* **1902**, *323*, 246−257.
(132) Kistiakowsky, G. B.; Sauer, K. Reactions of Methylene. 2. Ketene and Carbon Dioxide. *J. Am. Chem. Soc.* **1958**, *80*, 1066−1071.
(133) Aida, K.; Hirao, M.; Funabashi, A.; Sugimura, N.; Ota, E.; Yamaguchi, J. Catalytic reductive ring opening of epoxides enabled by zirconocene and photoredox catalysis. *Chem* **2022**, *8*, 1762−1774.
(134) Huang, C.; Ma, W.; Zheng, X.; Xu, M.; Qi, X.; Lu, Q. Epoxide Electroreduction. *J. Am. Chem. Soc.* **2022**, *144*, 1389−1395.
(135) Kantorowski, E. J.; Kurth, M. J. Expansion to Seven-Membered Rings. *Tetrahedron* **2000**, *56*, 4317−4353.
(136) Polanyi, M.; Szabo, A. L. On the mechanism of hydrolysis. The alkaline saponifications of amyl acetate. *Trans. Faraday Soc.* **1934**, *30*, 508.
(137) Davies, A. G.; Kenyon, J. Alkyl−oxygen heterolysis in carboxylic esters and related compounds. *Q. Rev., Chem. Soc.* **1955**, *9*, 203−228.

https://doi.org/10.1021/acs.jpcc.3c08356
J. Phys. Chem. C XXXX, XXX, XXX−XXX